Available online at www.sciencedirect.com
SCIENCE DIRECT®
Journal of Power Sources 145 (2005) 399–406
JOURNAL OF POWER SOURCES
www.elsevier.com/locate/jpowsour

Simplified evaluation of PEM-fuel cells by reduction of measurement parameters and using optimised measurement algorithms

M. Purmann *, Z. Styczynski [1]

Institute for Power Systems, University of Magdeburg, PO Box 4120, 39016 Magdeburg, Germany

Accepted 3 February 2005
Available online 4 May 2005

Abstract

PEM-fuel cells operated with hydrogen and air offer promising possibilities for the decentralised energy supply in stationary and mobile applications. But, there is still a remarkable need for more research for the optimisation of the single components even though the research, especially the development of membrane-electrode units and bipolar plates, has made considerable progress within recent years. This also applies to the definition of suitable test algorithms and parameters for recording the characteristics as well as long time tests.

The investigations for single cells or stacks can thereby be subdivided into investigations in the stationary and the dynamic state. This paper shows a simplified approach for the evaluation and modelling of PEM-fuel cell stacks for the stationary state. Based on the definition of regression approaches for the dependence of several parameters the number of stack parameters is initially reduced to a sufficient number of values. The remaining parameters are used to form an energy model which can be combined with the energy models of auxiliary components like air compressors and sinus inverters [1].

Algorithms for recording the parameters still have to be defined. Therefore, the tests for the preparation of a set of characteristic curves can be very time consuming because of the multitude of variable parameters. This paper presents and discusses optimised measurement algorithms for the evaluation of PEM-fuel cell stacks to reduce this time exposure.

Keywords: Fuel cell; Measurement parameter; Measurement algorithm; Energy model

1. Introduction

A fuel cell facility for stationary power generation consists of a multitude of components in addition to the stack. These components are: reformers, if fuel processing is necessary, as well as control sinus inverters, pumps and compressors for transporting the process media. An optimal adaptation of the operating points of the several components to the fuel cell is extremely important for fuel cell facilities in the lower power range.

The operational behaviour of the several components is important for adaptation. For evaluation of the operational behaviour of PEM-fuel cells numerous models exist which more or less satisfactorily describe the behaviour of the fuel cell. These models normally require a lot of characteristic variables which are not known if a commercial stack is used. For first considerations energy models are sufficient which do not require a detailed knowledge about the investigated fuel cell stack. However, the energy balance of a fuel cell is characterised by a larger number of variables as opposed to peripheral components like pumps or compressors which can be described with only a few parameters.

To describe the fuel cell energy balance the parameters of the process media on the inlet and the outlet of the stack as well as the voltage–current behaviour dependent on the parameters of the process media has to be known. The set of parameters can still be simplified by making some assumptions without remarkable information losses regarding the

* Corresponding author. Tel.: +49 391 6711092; fax: +49 391 6712408.
E-mail addresses: mathias.purmann@et.uni-magdeburg.de (M. Purmann), sty@et.uni-magdeburg.de (Z. Styczynski).
[1] Tel.: +49 391 6718866; fax: +49 391 6712408.

0378-7753/$ – see front matter © 2005 Elsevier B.V. All rights reserved.
doi:10.1016/j.jpowsour.2005.02.042

Nomenclature

A	area (cm^2)
b	Tafel parameter (mV)
c_p	specific heat capacity at constant pressure ($J\,kg^{-1}\,K^{-1}$)
C_S	radiation of the black radiator ($5.77\,W\,m^{-2}\,K^{-4}$)
C_W	specific heat capacity of water in the liquid state ($J\,kg^{-1}\,K^{-1}$)
d	characteristic diameter
F	Faraday constant ($96{,}485\,C\,mol^{-1}$)
g	acceleration of gravity ($9.81\,m\,s^{-2}$)
Gr	Grashof number (–)
h	specific enthalpy ($J\,kg^{-1}$)
$\dot{H}$	enthalpy flow ($J\,s^{-1}$)
$\dot{H}_B$	upper heating value flow ($J\,s^{-1}$)
i	current density ($mA\,cm^{-2}$)
i_0	exchange current density ($mA\,cm^{-2}$)
I	electric current (A)
k	thermal transmission coefficient ($W\,K^{-1}\,m^{-2}$)
l	characteristic length (m)
$\dot{m}$	mass flow ($g\,s^{-1}$)
M	molar mass ($g\,mol^{-1}$)
n	moles of exchanged electrons per mole of the fuel ($mol\,mol^{-1}$)
Nu	Nusselt number (–)
p	pressure (bar)
P	power (W)
Pr	Prandtl number (–)
$\dot{Q}$	heat flow ($J\,s^{-1}$)
r	evaporation heat ($J\,kg^{-1}$)
R	specific ohmic resistance ($\Omega\,cm^2$)
Re	Reynolds number (–)
t	temperature (°C)
T	temperature (K)
U	voltage (V)
$\dot{V}$	volume flow ($l\,min^{-1}$)
w	velocity ($m\,s^{-1}$)
x	absolute humidity ($kg\,kg^{-1}$)

Greek symbols

α	heat transfer coefficient ($W\,m^{-2}\,K^{-1}$)
β	volume expansion coefficient (–)
ε	emission ratio (–)
θ	position of the surface (–)
λ	heat conduction resistance ($W\,m^{-1}\,K^{-1}$)
ν	kinematic viscosity of the flowing substance ($m^2\,s^{-1}$)
ν	process gas utilisation (%)
ρ	density ($kg\,m^{-3}$)
τ	time (s)
φ	relative humidity (–)

Subscript

amb	ambient
air	air
ce	cell
conv	convection
cons	consumption
cw	cooling water
FC	fuel cell
forc	forced convection
free	free convection
H_2	hydrogen
in	inlet
loss	losses
max	maximum
out	outlet
rad	radiation
rev	reversible
s	saturation
St	steam

obtained simulation results. Such a simplified model will be presented in the following paragraphs.

2. Test equipment

The experimental application for the investigations can be seen in Fig. 1. The fuel cell test bench is equipped with a programmable logic controller which overtakes the control and safety tasks.

For the definition of the measurement algorithms and the acquisition of the measurement values a PC with the necessary data acquisition and the measurement application was installed.

The electronic load was controlled by the PC and a function generator Agilent 33120 A. The graphical environment

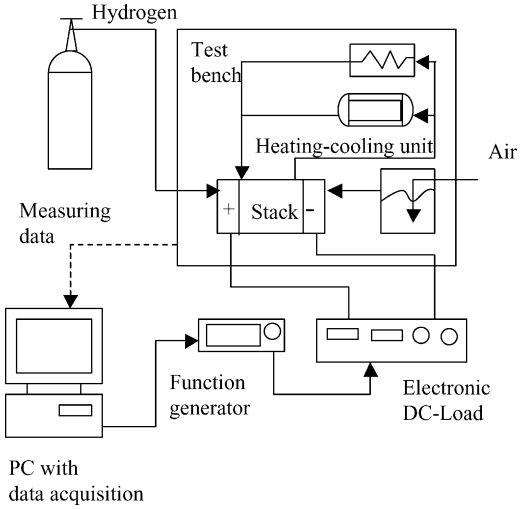

Fig. 1. Test application for the experimental investigations.

VEE Pro® was used to define the measurement algorithms. To prepare the fuel cell model a stack was measured from the open circuit operation to the point of rating at variation of the process parameters.

The appropriate measurements like stack voltage, temperatures, pressures, humidifier temperatures as well as hydrogen and air utilisation were acquired over a time period of 1 min at current steps of 1 A. The hydrogen utilisation was changed between 40 and 60% in 10% steps, the air utilisation from 10 to 25% in 5% steps, the stack temperature from 40 to 65 °C in 5 °C steps and the air humidifier temperature was changed by 2 °C steps.

3. Fuel cell model

3.1. Model of the U–I-characteristic

The characteristic of a PEM-fuel cell can be subdivided into three characteristic areas.

If only the two technically relevant areas are considered the characteristic can be emulated with the following empirical approach [1,2]:

$$U_{ce} = U_0 - b \ln i - Ri \quad (1)$$

with

$$U_0 = U_{rev} + b \ln i_0 \quad (2)$$

where U_{rev} is the reversible cell potential and i_0 and b are Tafel parameters of the oxygen reaction [3]. The linear area of the characteristic is mainly influenced by the ohmic resistance R. This ohmic resistance contains the ohmic losses within the membrane, the activation resistance of the hydrogen oxidation reaction and the mass flow resistance on the oxygen electrode.

The approach can be used if the cells show the same behaviour over the whole operating range. The behaviour can be assumed for optimised and well-engineered stacks.

Fig. 2 shows the dependence of the stack voltage on the current for the investigated stack at different fuel cell temperatures.

Since the cells show a slightly different behaviour and the operating parameters could not be kept completely constant the different terms of the regression approach do not exactly reflect the single over-voltages. Furthermore, at different stack temperatures and higher air utilisation voltage drops can occur since a definite transport of the produced water cannot be ensured because of a low pressure drop. At higher temperatures and fitted air volume flows good or very good results can be achieved with the regression approach used.

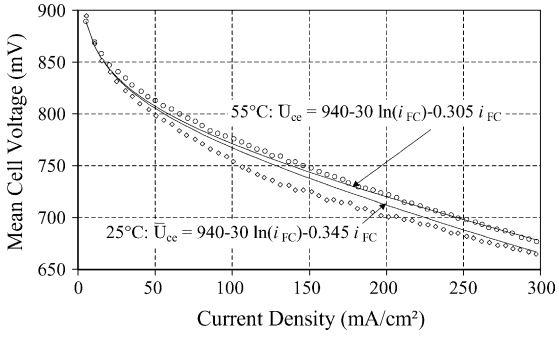

Fig. 2. *U–I* characteristic and determined regression at different stack temperatures (air utilisation 17%, hydrogen utilisation 50%).

3.2. Temperatures

The temperatures of the reactants on the respective outputs of the stack were measured with temperature sensors which belonged to humidity measurement equipment from the company Testo. These Ni10000 sensors were soldered together with the humidity sensor on a thread block. This block was screwed into a specially designed mounting which enabled the process gases to directly pass by the sensors.

Since the anode outlet, the outlet for the cooling water and the inlet for the cooling water are all situated on the same stack side it is useful to have a representation of the outlet temperature of hydrogen dependent on the outlet temperature of the cooling water and of the outlet temperature of the air dependent on the inlet temperature of the cooling water (Figs. 3 and 4). It could be noticed that there was a linear dependence of the cooling water temperatures and the outlet temperatures of the process gases which could be emulated by a linear regression approach.

During the measurement of the characteristics it could be observed that the outlet temperatures of the gases increased with increasing current density at constant air and hydrogen utilisation and constant stack temperature by approx. 1–2 K. This temperature change can be attributed to the imperfect insulation surrounding the temperature sensors since there were no remarkable temperature changes in dependence on air and hydrogen utilisation at nominal power or high volume

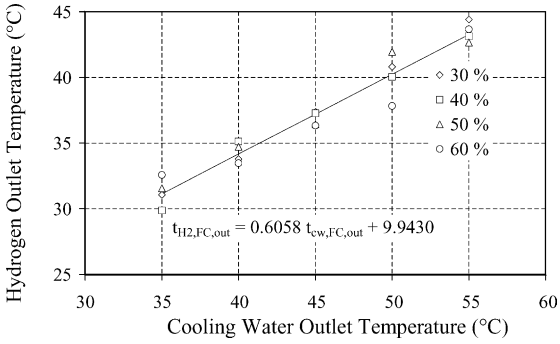

Fig. 3. Hydrogen outlet temperature dependent on the cooling water outlet temperature and the hydrogen utilisation.

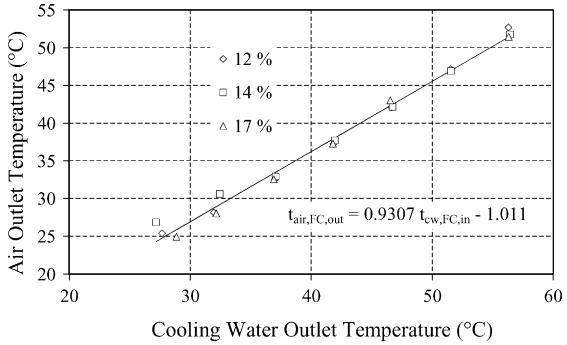

Fig. 4. Air outlet temperature dependent on the cooling water outlet temperature and the air utilisation.

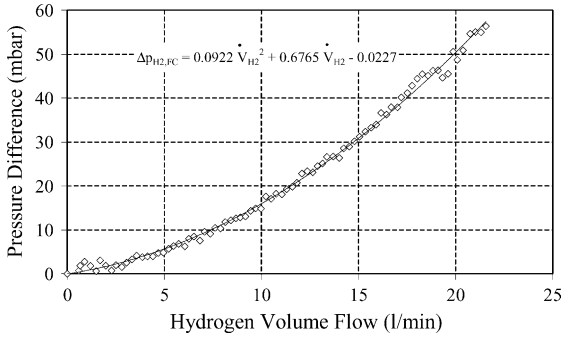

Fig. 5. Pressure losses on the anode side dependent on the hydrogen volume flow.

flow of the process media. For this reason the outlet temperatures on the anode are lower than on the outlet of the cathode because of the lower gas flow.

3.3. Pressure losses

The supplied air has to fulfil several tasks. Firstly, the oxygen is made available for the chemical reaction with the air transport. The oxygen concentration on the outlet is lower than on the inlet since the reactant is consumed via the length of the cathode channel. Lower oxygen concentration results in higher activation over-voltages and diffusion losses [4]. The decrease of concentration can be influenced by the stoichiometry number on a limited scale. The influence of the air flow on the oxygen concentration decreases with increasing stoichiometry number. The intermediate oxygen concentration in the air via the transport path amounts to 10% at a stoichiometry number of 1. A concentration of 15% is reached at a stoichiometry number of 2 and 17.5% is adequately reached with a number of 4.

Furthermore, the humidity share in the cell is regulated with air flow variation. The ability of air to transport water increases super-proportionally with increasing temperature. Additionally, the cathode air flow transports a higher amount of water with decreasing air utilisation and reaches the point of saturation via longer channel length [5].

Higher stoichiometry numbers at constant channel cross-section cause higher flow velocities and higher pressure losses. Simultaneously, the transport ability of the air volume flow at higher pressures is lower so that the problem of a dehumidified membrane at the air inlet at counter-flow of the reactants can be reduced at a defined air volume flow. Furthermore, with increasing pressure difference it is easier to remove the liquid water, which can be found inside the stack.

However, high pressure differences demand a high flow rate of the compressor and therewith a higher energy demand.

The design of the flow field has a large influence on the behaviour of the fuel cell characteristic and the electrical efficiency of the facility.

However, the abilities of the flow field design are also limited. For example, channels with narrow cross-sections can lead to non-uniform supplied zones or cells because of the larger pressure difference between inlet and outlet of the fuel cell stack [6]. Furthermore, the effectiveness of the reactant supply and the water removal are not only dependent on the geometric parameters like channel length and height, but also on the velocity of the entering gases [7].

If the stack is a commercial product and the flow field is therewith defined, only the volume flow dependent on the stack temperature and the stack power can be adapted. For this case the dependence of the pressure losses via the stack on the air and hydrogen flow has to be investigated (Figs. 5 and 6).

On the anode side there are normally lower pressure losses than on the cathode side since the volume flow of the hydrogen is by far lower than the air volume flow.

3.4. Heat losses

The heat losses between the stack and the surrounding environment are caused by convection and radiation.

The heat released via the stack surface by convection can be calculated with Eq. (3) if the heat transfer coefficient of the stack surface and the temperature difference between surroundings and surface are known [8]:

$$\dot{Q}_{\mathrm{FC,conv}} = \alpha A(t_{\mathrm{FC}} - t_{\mathrm{amb}}) \tag{3}$$

The convective heat transfer and therewith the heat transfer coefficient are influenced by a number of physical properties of the flowing medium. The most important parameters are

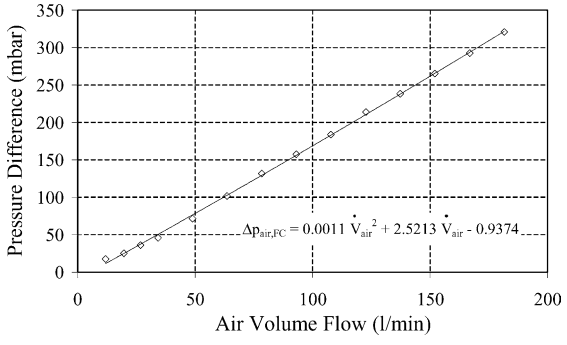

Fig. 6. Pressure losses on the cathode side dependent on the air volume flow.

the density, the specific heat capacity at constant pressure, the heat conductivity, the volume coefficient of expansion, the kinematic viscosity and the thermal diffusivity.

The heat transfer coefficient at free convection can be calculated from the Nusselt number, the heat conductivity of the flowing medium as well as the characteristic dimensions of the body [9]:

$$\alpha = \frac{Nu\lambda}{l} \tag{4}$$

The flow velocity is a result of the lifting power at free flow and the Nusselt number can be calculated from the Grashof- and the Prandtl-number:

$$Nu = \theta C(Gr\,\mathrm{Pr})^n \tag{5}$$

The constants C and n depend on $Gr\,Pr$ and θ considers the location of the surface. The Prandtl- and the Grashof-number are defined in the Eqs. (6) and (7):

$$\mathrm{Pr} = \frac{\nu}{a} \tag{6}$$

$$Gr = \frac{gl^3(t_{\mathrm{FC}} - t_{\mathrm{amb}})\beta}{\nu^2} \tag{7}$$

According to Zhukauskas the Nusselt number on horizontal tubes can be calculated with Eqs. (8) and (9) for the convective heat transfer and at free flow [10]:

$$Nu = 0.28\,Re^{0.6}\,Pr^{0.36}, \quad Re > 1000 \tag{8}$$

$$\mathrm{Re} = \frac{wd}{\nu} \tag{9}$$

If one presents the heat transfer coefficient for free and forced convection dependent on the temperature with the assumption that the heat transfer shows a similar behaviour to the convection on a cross passed tube it can be shown that the heat transfer coefficient for a forced convection shows only a slight change within the investigated temperature range and the coefficient for the free convection only slightly increases from a temperature difference of approx. 4–5 K.

It can also be assumed that the heat losses caused by convection increase nearly proportionally with the increasing temperature difference (Fig. 7).

The stack used in this study contains neither a cross-flow against a tube nor an ideally passed body.

Furthermore, the stack is connected in a heat conducting manner via the mounting and the media and current supporting tubes to the surroundings.

An experimental investigation of the heat losses via the stack surface is necessary.

The heat losses which are caused by the heat radiation can be calculated with the following approach:

$$\dot{Q}_{\mathrm{FC,rad}} = A_{\mathrm{FC}}\varepsilon_{\mathrm{FC,amb}}C_{\mathrm{S}}\left[\left(\frac{T_{\mathrm{FC}}}{100}\right)^4 - \left(\frac{T_{\mathrm{amb}}}{100}\right)^4\right] \tag{10}$$

where $\varepsilon_{\mathrm{Bz,amb}}$ is the resulting emission ratio between the fuel cell surface and the surfaces of the surroundings.

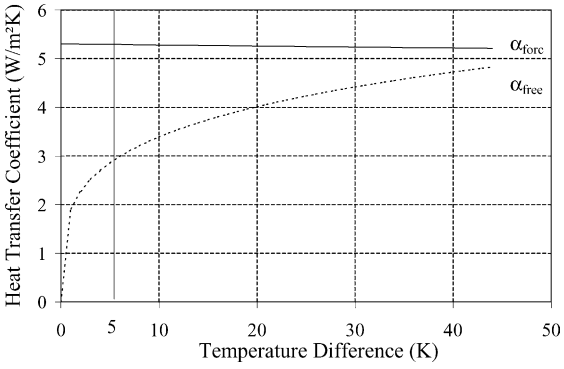

Fig. 7. Calculated heat transfer coefficient at free and forced convection dependent on the stack temperature (ambient temperature 25 °C).

The losses of heat radiation are nearly linearly dependant on the stack temperature (Fig. 8) and have nearly the same value as the convection losses if a constant temperature of the surrounding surfaces and low fuel cell temperatures can be assumed.

In principle there are two possible experimental approaches for evaluating the heat losses via the fuel cell surface. In the first case the stack is heated and kept at a defined temperature while the gas supply is switched off and the released heat flow is measured via the stack inlet and outlet temperatures as well as the volume flow of the heating water. This method was only minimally suitable since the temperature difference of the cooling flow on the inlet and outlet of the stack was very low. This low temperature difference resulted in strongly changing values for the calculated heat flow.

For getting some reliable results the heat flow was measured 10 times for 15 min at defined stack temperatures and the mean value and the standard deviation were determined afterwards.

The second and better possibility is to record the cooling down curve and calculate the heat losses with the recorded temperature curve and the heat capacity of the stack.

For these investigations the stack was heated up to a temperature of 70 °C and after the heat supply the temperature of

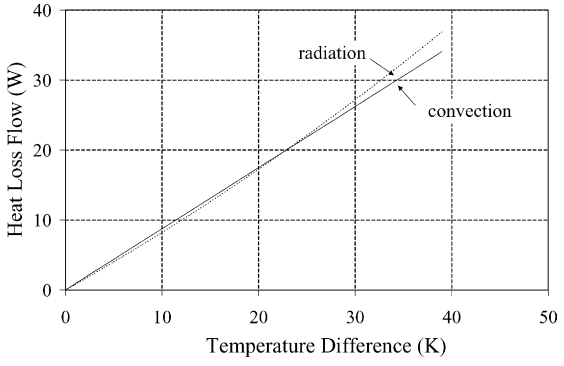

Fig. 8. Calculated heat loss flow caused by radiation and convection losses dependent on the stack temperature (ambient temperature 25 °C, emission coefficient 0.76, heat transfer coefficient 5.2 W m^{-2} K).

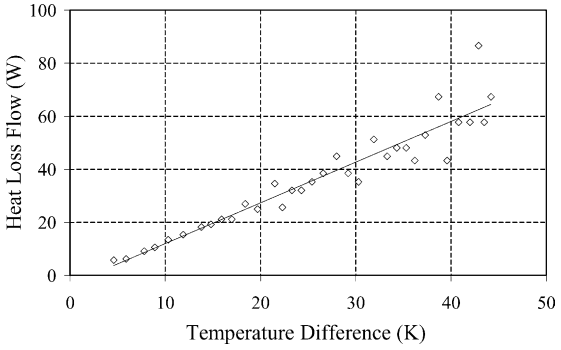

Fig. 9. Heat loss flow dependent on the temperature difference determined from the cooling down curve.

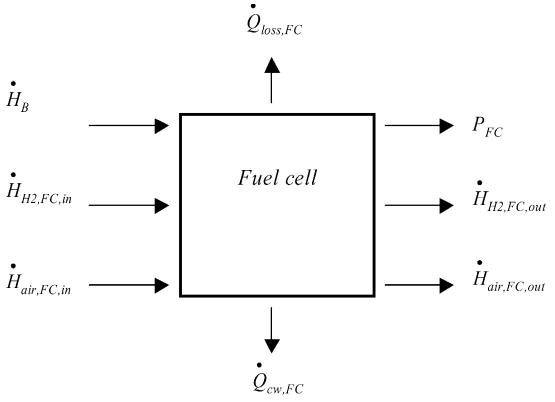

Fig. 10. Energy flows of the stack.

the stack was measured at defined time intervals. The ambient temperature was approx. 23 °C and only slightly increased during the experiment to 24 °C. The heat capacity of the fuel cell could be defined with 0.68 kg kg^{-1} K^{-1} based on the known volume shares of the single stack components and the respective specific heat capacities and densities.

Starting with an assumed linear temperature decrease in the time intervals the heat losses can be evaluated dependent on the change of the temperature difference between stack and surroundings and related to the time interval:

$$\dot{Q}_{\mathrm{FC,loss}} = \frac{m_{\mathrm{FC}} c_{\mathrm{FC}} \Delta(t_{\mathrm{FC}} - t_{\mathrm{amb}})}{\Delta\tau} \tag{11}$$

As the calculations for the heat losses of the stack separated into convection and heat radiation denote there is an almost linear dependence of the heat loss flow on the temperature difference (Fig. 9).

The comparison of the heat losses acquired from the cooling curve of the stack and calculated from the heat flow transported by the cooling water shows a correlation of the values of both methods [11].

The corresponding regression line can then be calculated with Eq. (12):

$$\dot{Q}_{\mathrm{FC,loss}} = \left[-2.571 + 1.51\left(\frac{t_{\mathrm{cw,FC,out}} + t_{\mathrm{cw,FC,in}}}{2} - t_{\mathrm{amb}}\right)\right] \tag{12}$$

3.5. Energy balance

For the energy balance a total of eight energy fluxes have to be recorded which are represented in Fig. 10.

The hydrogen is supplied to the stack in nearly dry state if the humidifier is switched off. The corresponding enthalpy flow can be calculated with Eq. (13) if the standard volume flow, the temperature and the pressure on the inlet of the anode are measured:

$$\dot{H}_{\mathrm{H_2,FC,in}} = \dot{V}_{\mathrm{H_2,FC,in}}\, \rho_{\mathrm{H_2,FC,in}}\, c_{p,\mathrm{H_2,FC,in}}\, t_{\mathrm{H_2,FC,in}} \tag{13}$$

The mass flow of consumed hydrogen is directly proportional to the current if the gas crossover is neglected and can be calculated with Eq. (14):

$$\dot{m}_{\mathrm{H_2,FC,cons}} = \frac{IM_{\mathrm{H_2}}}{2F} \tag{14}$$

The enthalpy flow coming from the outlet of the anode can be calculated via the mass balance:

$$\begin{aligned}\dot{H}_{\mathrm{H_2,FC,out}} = {} & (\dot{m}_{\mathrm{H_2,FC,in}} - \dot{m}_{\mathrm{H_2,FC,cons}}) \\ & \times [c_{p,\mathrm{H_2,FC,out}} t_{\mathrm{H_2,FC,out}} \\ & + x_{\mathrm{H_2,FC,out}} (r_{0,\mathrm{FC,out}} \\ & + c_{p,\mathrm{St,FC,out}} t_{\mathrm{H_2,FC,out}})]\end{aligned} \tag{15}$$

Beside the sensitive heat the evaporated heat is also considered in the enthalpy flow.

The demand of chemical energy can be calculated via the theoretical cell voltage (voltage related to the upper heating value) or the demanded hydrogen mass flow and the upper heating value:

$$\dot{H}_{\mathrm{B}} = \dot{m}_{\mathrm{H_2,FC,cons}} h_0 \tag{16}$$

The provided air which is transported through the humidifier can be considered nearly saturated.

The enthalpy of the gas–steam mix results from the sum of the enthalpies of the mixture ingredients:

$$\begin{aligned}\dot{H}_{\mathrm{air,FC,in}} = {} & \dot{V}_{\mathrm{air,FC,in}} \rho_{\mathrm{air,in}} \times [c_{p,\mathrm{air,FC,in}} t_{\mathrm{air,FC,in}} \\ & + x_{\mathrm{s,FC,in}} (r_{0,\mathrm{FC,in}} + c_{\mathrm{p,St,FC,in}} t_{\mathrm{air,FC,in}})]\end{aligned} \tag{17}$$

The parameters of the air and steam like density and heat capacity can be calculated from regression approaches which are available in literature sources.

The vapour pressure which is necessary for determining the absolute humidity and is dependant on the temperature can be also calculated from a regression approach or by using the Antoine-equation.

With the relative humidity and the vapour pressure the share of humidity in the air can be determined:

$$x = 0.622 \frac{\varphi p_{\mathrm{s}}}{p - \varphi p_{\mathrm{s}}} \tag{18}$$

The enthalpy flow at the cathode outlet can now be calculated since the amount of water supplied via fresh air as well as the amount of water produced by the chemical reaction is known and the humidity levels at the outlet of the electrodes have been measured. The water removed from the electrode is not completely gaseous. For this reason a term has to be provided in the equation which considers the liquid share of water in the waste air:

$$\dot{H}_{\mathrm{air,FC,out}} = \dot{m}_{\mathrm{air,FC,out}}[c_{p,\mathrm{air,FC,out}} t_{\mathrm{air,FC,out}} + x_{\mathrm{air,FC,out}}(r_{0,\mathrm{FC,out}} + c_{p,\mathrm{St,FC,out}} t_{\mathrm{air,FC,out}}) + (x_{\mathrm{air,FC,max}} - x_{\mathrm{air,FC,out}}) c_{\mathrm{w}} t_{\mathrm{air,FC,out}}] \quad (19)$$

The specific heat capacity of the waste air is now calculated from the mixture ratio of oxygen and nitrogen.

This mixture ratio is also considered for the calculation of the absolute humidity since the specific gas constant of the waste air is slightly smaller than the constant of the fresh air. Beside the heat losses the final parameter of the power has to be calculated for the energy balance:

$$P_{\mathrm{FC}} = U_{\mathrm{FC}} I_{\mathrm{FC}} \quad (20)$$

The heat flow of the cooling water result from Eq. (21):

$$\dot{Q}_{\mathrm{cw,FC}} = \dot{H}_{\mathrm{B}} + \dot{H}_{\mathrm{H_2,FC,in}} + \dot{H}_{\mathrm{air,FC,in}} - \dot{H}_{\mathrm{H_2,FC,out}} - \dot{H}_{\mathrm{air,FC,out}} - P_{\mathrm{FC}} - \dot{Q}_{\mathrm{FC,loss}} \quad (21)$$

The exemplary results of the measured and calculated cooling water flow for the carried out measurements are presented in Figs. 11 and 12 for a stack temperature of approx. 55 and 45 °C, a hydrogen utilisation of 50% as well as an air utilisation of 17 and 14%, respectively, and an air inlet temperature of 22 and 26 °C, respectively.

The dew point of the fresh air is also situated at these temperatures. The calculated cooling heat flow is based on the aforementioned approaches. The measured cooling heat flow was interpolated with a regression approach of second order. The graphs of the calculated and measured cooling heat flow are nearly congruent and support the proposed approach as well as the metering precision of the single sensors.

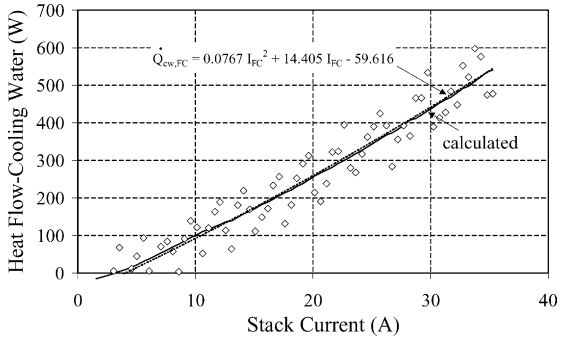

Fig. 11. Calculated and measured heat flow via the cooling water (stack temperature 45 °C, hydrogen utilisation 50%, air utilisation 17%, air inlet temperature 26 °C).

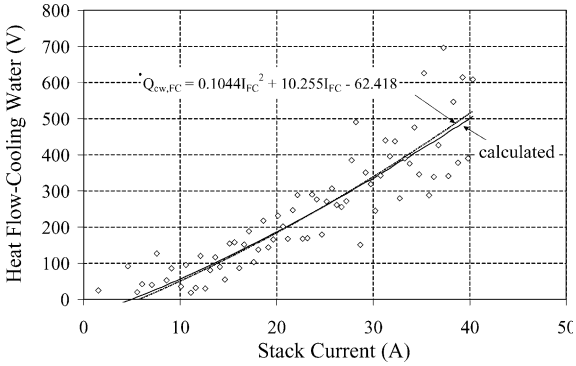

Fig. 12. Calculated and measured heat flow via the cooling water (stack temperature 55 °C, hydrogen utilisation 50%, air utilisation 14%, air inlet temperature 22 °C).

3.6. Comparison of model and realistic behaviour

The applicability of the simplifications still has to be proven since a reduced set of parameters with single values was used.

Figs. 13 and 14 show the calculated cooling heat flow and the regression of the measured cooling heat flow for both presented cases.

The tolerance of both heat flows ranges from approx. 2 to 5 up to 200% whereby the absolute failure does not amount to more than 10 W.

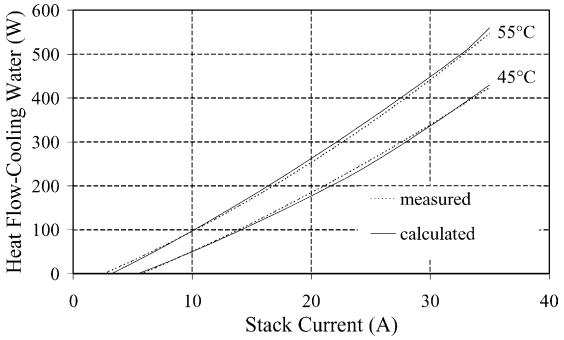

Fig. 13. Modelled heat flow via the cooling water based on the data set from Table 1 and heat flow interpolated from measured data.

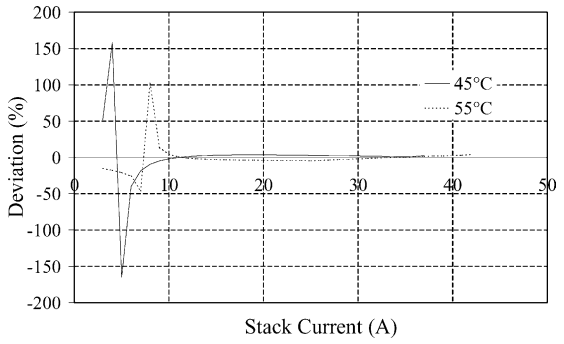

Fig. 14. Relative deviation of measured and calculated heat flow via the cooling water.

Table 1
Reduced parameter set

Stack temperature (°C)	45	55
Hydrogen inlet temperature $t_{H_2,FC,in}$ (°C)	25	25
Hydrogen inlet humidity $\varphi_{H_2,FC,in}$	0	0
Hydrogen outlet humidity $\varphi_{H_2,FC,out}$	0.82	0.3
Hydrogen utilisation ν_{H_2} (%)	50	50
Air inlet temperature $t_{air,FC,in}$ (°C)	22	26
Air inlet humidity $\varphi_{air,FC,in}$	1	1
Air outlet humidity $\varphi_{air,FC,out}$	0.82	0.78
Air utilisation ν_{air} (%)	17	14
Regression parameter for the characteristic		
Cell voltage U_{ce}	958.7	981.2
Tafel parameter b (mV)	33.277	34.157
Internal resistance R ($\Omega\,cm^2$)	0.2780	0.3039

The reduced parameter set for the fuel cell investigated in the paper is presented in Table 1.

4. Conclusion

If the operation of a PEM-fuel cell is considered under stationary conditions with the characteristics of a fuel cell, the energy balance can be described with a relatively low number of data. The heat losses on the stack surface, the pressure losses, the stack outlet temperatures and the characteristic can be simulated by using regression approaches. The use of these regression approaches result in a reduced set of parameters.

The inlet temperatures, the humidity levels of the process gases, the stack temperature as well as the volume flows and the humidity levels on the outlet of the stack form the set of necessary parameters. With the mentioned regression approaches and parameters the energy flows can now be calculated. The results reflect the energy balance and the energy flows on the interfaces to the surroundings in an adequate manner. This can be used in combination with energy models of the peripheral components.

References

[1] Y.W. Rho, O.A. Velev, S. Srinivasan, J. Electrochem. Soc. 141 (1994) 2084–2088.
[2] Y.W. Rho, S. Srinivasan, J. Electrochem. Soc. 141 (1994) 2089–2096.
[3] J. Kim, S. Lee, S. Srinivasan, J. Electrochem. Soc. 142 (1995) 2670–2675.
[4] M.L. Perry, J. Newman, E.J. Cairns, J. Electrochem. Soc. 145 (1998) 5–15.
[5] Z. Ogumi, Z. Takehara, S. Yoshizawa, J. Electrochem. Soc. 131 (1984) 769–773.
[6] D. Thirumalai, R.E. White, J. Electrochem. Soc. 144 (1997) 1717–1723.
[7] H. Dohle, A. Kornyshev, A. Kulikovsky, J. Mergel, D. Stolten, Electrochem. Commun. (3) (2001) 73–80.
[8] G. Meyer, E. Schiffner, Technische Thermodynamik, VEB Fachbuchverlag, Leipzig, 1989.
[9] H. Effenberger, Dampferzeuger, VEB Deutscher Verlag für Grundstoffindustrie, Leipzig, 1987.
[10] J. Schmidt, H. Boye, A. Mahrle, Arbeitsheft Wärmeübertragung, Otto-von-Guericke Universität, Magdeburg, 1992.
[11] M. Purmann, Simulation des stationären Verhaltens von PEM-Brennstoffzellen, in: Proceedings of the Fachtagung Elektrische Energiewandlungssysteme des Instituts für Elektrische Energiesysteme, Magdeburg, 13–14 March, 2001, pp. 47–52.